FLOW AND HEAT TRANSFER IN CROSS-STREAM TYPE T-JUNCTIONS: A COMPUTATIONAL STUDY

Benjamin Krumbein[1*], Suad Jakirlić[1*], Vincenzo Termini[1], Anna Mizobuchi[1,2], Cameron Tropea[1]

[1] Institute of Fluid Mechanics and Aerodynamics, Technische Universität Darmstadt
Allarich-Weiss-Straße 10, 64287 Darmstadt, Germany.
[2] Department of Mechanical Engineering, Keio University
Hiyoshi 3-14-1, Kohoku-ku, Yokohama 223-8522, Japan.
*Corresponding authors: krumbein@sla.tu-darmstadt.de, s.jakirlic@sla.tu-darmstadt.de

ABSTRACT

The present computational study is concerned with the thermal mixing of flow-crossing streams in a T-shaped junction, focussing primarily on a configuration subjected to temperature dependent fluid property conditions. The reference experimental investigation is conducted by Hirota *et al.* (2010). Preliminary, a quasi-two dimensional configuration with constant fluid properties, for which the reference DNS (Direct Numerical Simulation) database is made available by Hattori *et al.* (2014), is simulated. The presently applied computational model is based on a VLES (Very Large Eddy Simulation) formulation of Chang *et al.* (2014). The residual turbulence is modeled employing the RANS-based (Reynolds-Averaged Navier-Stokes) elliptic-relaxation eddy viscosity model of Hanjalić *et al.* (2004). In addition to the VLES, both flow configurations are computed applying the background RANS model representing the constituent of the VLES method. Whereas the eddy viscosity model describes fully-modeled turbulence in the RANS framework, it relates to the unresolved sub-scale turbulence within the VLES methodology. Unlike the RANS method, the VLES method is capable of capturing the spectral dynamics of turbulence to an extent complying with the underlying grid resolution. The results obtained with the present VLES model follow closely the reference DNS data in the Hattori *et al.* (2014) case. In the more complex Hirota *et al.* (2010) configuration, the flow field is captured reasonably well, while the computationally obtained thermal fields suggest a more intensive mixing relative to the reference experiment.

INTRODUCTION

Flow phenomena encountered during the turbulent mixing of two streams crossing in a T-shaped junction are of interest for a variety of practical applications. While T-junctions can be found in many technical systems in the chemical and petroleum industry, major focus in recent years has been on their application in cooling systems of nuclear power plants. Several experimental and computational studies have focused on this topic, with the goal to more accurately predict thermal fatigue due to cyclic temperature fluctuations induced by the mixing process (see e.g. Walker *et al.* (2009), Kuczaj *et al.* (2010), Kim & Jeong (2012)). Furthermore, T-junctions are relevant for automotive applications, including HVAC (heating, ventilation and air-conditioning) units (Hirota *et al.*, 2010) as well as exhaust systems.

The present study is concerned with the turbulent mixing and heat transfer in two T-junction configurations: First, a quasi-two-dimensional configuration (i.e. infinite extension in spanwise direction) with constant fluid properties is investigated. The geometry and flow conditions for this case comply with the reference DNS study by Hattori *et al.* (2014). Secondly, a full three-dimensional configuration with variable flow properties is considered, which was studied experimentally by Hirota *et al.* (2010). Fig. 1 shows a schematic depiction of the geometry. In both cases the flow is characterized by two turbulent streams of different temperatures issuing from the horizontal main channel/duct ('cold stream' at T_c) and a vertically positioned branch channel/duct ('hot stream' at T_h). In the quasi-two-dimensional case, the side walls are replaced by planes with periodic boundary conditions in order to model the infinite extension in spanwise direction. The height of the branch channel is equal to the main channel height ($B = H$). The flow issuing from the inlet channels matches fully developed channel flow at a Reynolds number of $\mathrm{Re_b} = 5650$ based on the bulk-velocity U_b and the channel height H (corresponding to a friction Reynolds number of $\mathrm{Re}_\tau = 180$). The Prandtl number is $\mathrm{Pr} = 0.71$. In the three-dimensional case, the branch ducts height is $B = H/2$ and the spanwise dimension equates to $A = 2H$, with $H = 60\,\mathrm{mm}$ in the experimental set-up of Hirota *et al.* (2010). The Reynolds numbers are $\mathrm{Re_b} = U_b d_h/\nu \approx 15000$ in the main duct and $\mathrm{Re_b} \approx 9000$ in the branch duct. Here, d_h denotes the respective hydraulic diameter and U_b the bulk velocity equal in both channels. In the experimental investigations, air was used and the bulk temperatures were set to $T_c = 12^\circ\,\mathrm{C}$ and $T_h = 60^\circ\,\mathrm{C}$.

The unsteady flow conditions stemming from the turbulent mixing as well as flow features such as separation and reattachment are difficult to predict by classical (U)RANS models. In this work, a seamless hybrid LES/RANS model proposed by Chang *et al.* (2014), derived in line with the VLES concept of Speziale (1998), is employed. The elliptic-relaxation eddy viscosity model of Hanjalić *et al.* (2004), denoted as ζ-f model, is used to describe the unresolved turbulence motion. In addition, both flow configuration are computed within the classical (U)RANS framework, applying the aforementioned ζ-f model. The computational results including mean values and turbulence statistics obtained with the present VLES and RANS models are analyzed along with the respective reference DNS and experimental data base.

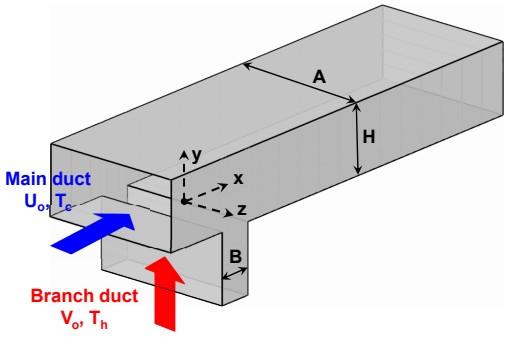

Figure 1. Schematic of the flow configuration considered.

COMPUTATIONAL METHODOLOGY

In the present VLES framework, the flow field is obtained by solving the Favre-averaged continuity and momentum equations for a variable density Newtonian fluid, given by

$$\frac{\partial \overline{\rho}}{\partial t} + \frac{\partial}{\partial x_i}(\overline{\rho}\widetilde{U}_i) = 0 \tag{1}$$

and

$$\frac{\partial}{\partial t}\left(\overline{\rho}\widetilde{U}_i\right) + \frac{\partial}{\partial x_j}\left(\overline{\rho}\widetilde{U}_i\widetilde{U}_j\right) = -\frac{\partial \widetilde{p}}{\partial x_i} + \frac{\partial}{\partial x_j}\left\{\mu\left[\left(\frac{\partial \widetilde{U}_i}{\partial x_j} + \frac{\partial \widetilde{U}_j}{\partial x_i}\right) - \frac{2}{3}\delta_{ij}\frac{\partial \widetilde{U}_k}{\partial x_k}\right] - \tau_{ij}\right\}, \tag{2}$$

with the velocity components U_i, the pressure p, the density ρ, the dynamic viscosity μ and the Kronecker delta δ_{ij}. The tilde operator denotes the Favre averaging ($\widetilde{\Phi} = \overline{\rho\Phi}/\overline{\rho}$) and $\tau_{ij} = \overline{\rho}(\widetilde{U_i U_j} - \widetilde{U}_i\widetilde{U}_j)$ represents the stress tensor associated with the sub-grid motion, which has to be modeled. The temperature is obtained by solving the Favre-averaged energy equation, where viscous dissipation is neglected in this work due to the low Mach numbers considered:

$$\frac{\partial}{\partial t}\left(\overline{\rho}c_p\widetilde{T}\right) + \frac{\partial}{\partial x_i}\left(\overline{\rho}\widetilde{U}_i c_p\widetilde{T}\right) = \frac{\partial}{\partial x_i}\left(\lambda\frac{\partial \widetilde{T}}{\partial x_i} - q_i\right). \tag{3}$$

Here, T is the temperature, c_p the specific heat at constant pressure, $\lambda = c_p\mu/Pr$ the thermal conductivity and $q_i = \overline{\rho}c_p(\widetilde{U_i T} - \widetilde{U}_i\widetilde{T})$ the sub-grid turbulent heat flux determined by the turbulence model. Temperature dependence of the dynamic viscosity is considered by employing Sutherland's formula (Sutherland, 1893):

$$\mu(\widetilde{T}) = \frac{A_s\sqrt{\widetilde{T}}}{1 + T_s/\widetilde{T}}. \tag{4}$$

Density is evaluated by applying the ideal gas law $\overline{\rho} = \overline{p}/(R\widetilde{T})$, with the specific gas constant R. The specific heat c_p is kept constant.

In order to close the system of equations, the residual stress tensor τ_{ij} and the residual turbulent heat flux q_i have to be modeled. The former is modeled by applying the Boussinesq assumption, which linearly relates the residual stresses to the filtered rate of strain tensor $\widetilde{S}_{ij}$, leading to

$$\tau_{ij} = -2\mu_t\widetilde{S}_{ij} - \frac{1}{3}\tau_{kk}\delta_{ij}. \tag{5}$$

The eddy viscosity μ_t is calculated in line with the proposal of Speziale (1998) as $\mu_t = F_r\mu_t^{\mathrm{RANS}}$, where μ_t^{RANS} is the eddy viscosity predicted by the underlying RANS model, based on the unsteady flow field and F_r is the 'resolution function' damping the influence of the RANS model, depending on the local mesh resolution. Applying the ζ-f model, an elliptic-relaxation-based eddy viscosity model of Hanjalić *et al.* (2004), as the underlying RANS model, the VLES eddy viscosity is defined as

$$\mu_t = F_r\,\overline{\rho}\,C_\mu^\zeta\,\zeta_{us}\,T_{us} \tag{6}$$

Here, the $(\cdot)_{us}$ quantities are determined by the RANS-based subscale model, which solves equations for the turbulent kinetic energy k_{us} and its dissipation rate ε_{us} as well as the variable ζ_{us} ($= \overline{v^2}_{us}/k_{us}$), representing a measure for the wall-normal turbulent intensity and the elliptic function f_{us}. The model transport equations in variable density formulation read:

$$\frac{\partial}{\partial t}(\overline{\rho}k_{us}) + \widetilde{U}_j\frac{\partial}{\partial x_j}(\overline{\rho}k_{us}) = P_k - \overline{\rho}\varepsilon_{us} + \frac{\partial}{\partial x_j}\left[\left(\mu + \frac{\mu_t}{\sigma_k}\right)\frac{\partial k_{us}}{\partial x_j}\right], \tag{7}$$

$$\frac{\partial}{\partial t}(\overline{\rho}\varepsilon_{us}) + \widetilde{U}_j\frac{\partial}{\partial x_j}(\overline{\rho}\varepsilon_{us}) = \frac{C_{\varepsilon_1}P_k - C_{\varepsilon_2}\overline{\rho}\varepsilon_{us}}{T_{us}} + \frac{\partial}{\partial x_j}\left[\left(\mu + \frac{\mu_t}{\sigma_\varepsilon}\right)\frac{\partial \varepsilon_{us}}{\partial x_j}\right], \tag{8}$$

$$\frac{\partial}{\partial t}(\rho\zeta_{us}) + \widetilde{U}_j\frac{\partial}{\partial x_j}(\overline{\rho}\zeta_{us}) = \overline{\rho}f_{us} - \frac{P_k}{k_{us}}\zeta_{us} + \frac{\partial}{\partial x_j}\left[\left(\mu + \frac{\mu_t}{\sigma_\zeta}\right)\frac{\partial \zeta_{us}}{\partial x_j}\right], \tag{9}$$

$$L_{us}^2\nabla^2(\overline{\rho}f_{us}) - \overline{\rho}f_{us} = \frac{1}{T_{us}}\left(\overline{\rho}C_1 + C_2\frac{P_k}{\varepsilon_{us}}\right)\left(\zeta_{us} - \frac{2}{3}\right), \tag{10}$$

with the production rate $P_k = 2\mu_t\widetilde{S}_{ij}\widetilde{S}_{ij}$, the time scale

$$T_{us} = \frac{k_{us}}{\varepsilon_{us}} \tag{11}$$

and length scale

$$L_{us} = C_L\max\left[\frac{k_{us}^{3/2}}{\varepsilon_{us}}, C_\eta\left(\frac{\nu^3}{\varepsilon_{us}}\right)^{1/4}\right]. \tag{12}$$

The model coefficients are summarized in Table 1.

The 'resolution function' F_r in Eq. (6) provides a seamless blending between the DNS limit ($F_r \to 0$, $\mu_t \to 0$) and the RANS limit ($F_r \to 1$, $\mu_t \to \mu_t^{\mathrm{RANS}}$). Between these two limits an LES or VLES mode is recovered. The formulation of Chang *et al.* (2014) is adopted, which is based on the ratio of the grid spacing $\Delta = (\Delta_x\Delta_y\Delta_z)^{1/3}$ to the turbulent length scale $\Lambda_{us} = k_{us}^{3/2}/\varepsilon_{us}$:

$$F_r = \min\left[\left(\frac{\Delta}{\Lambda_{us}}\right)^{4/3}, 1\right]. \tag{13}$$

Finally, the non-resolved turbulent heat fluxes q_i are modeled applying the gradient diffusion hypothesis, resulting in

$$q_i = \frac{\mu_t c_p}{\mathrm{Pr}_t}\frac{\partial \widetilde{T}}{\partial x_i}, \tag{14}$$

with the turbulent Prandtl number set to $\mathrm{Pr}_t = 1$.

Table 1. Model coefficients in the present VLES model.

C_μ	C_{ε_1}	C_{ε_2}	C_1	C_2	σ_k	σ_ε	σ_ζ	C_L	C_η
0.22	$1.4(1+0.045/\sqrt{\zeta})$	1.9	0.4	0.65	1	1.3	1.2	0.36	85

The predictive capabilities of the present VLES model were preliminary explored by computing several generic and complex flow configurations including channel flow, flow over periodic hills, jet impingement onto a heated wall, vortex tubes and car aerodynamics. Interested readers are referred to Chang *et al.* (2014), Krumbein *et al.* (2016) and Jakirlić *et al.* (2016) for more details.

The described model is implemented in the open-source continuum mechanics library OpenFOAM®. Structured hexahedral meshes are used throughout. In line with standard practices for LES in the context of the finite volume method, second-order schemes are applied. Accordingly, the central differencing scheme is used for the spatial discretization of both the convective and diffusive term in the momentum equation. The convective term in the energy equation is discretized applying a total variation diminishing scheme. For time marching, the second-order backward differentiation formula is adopted.

CONSTANT PROPERTY FLOW IN A T-JUNCTION

In this quasi-two-dimensional configuration, density and viscosity are kept constant. Consequently, temperature is treated as a passive scalar, as it is the case in the reference DNS by Hattori *et al.* (2014). The computational domain for the T-junctions consists of two parts: the horizontal main channel with dimensions $8H \times H \times H$ and the vertical branch channel with dimensions $H \times H \times H$. The mesh consists of 278.460 cells in total, with $157 \times 45 \times 34$ cells in the main part and $45 \times 25 \times 34$ cells in the branch channel. Cells are refined towards top and bottom walls, applying a ratio of 10 for the spacing between coarsest and finest cell. Fully developed turbulent inflow data is generated by simultaneous precursor simulations and mapped to the inlet planes of the computational domain. Temperature at the inlets is set to constant values T_c and T_h. At the walls, no-slip boundary conditions are prescribed for the velocity, while an adiabatic condition is imposed for the temperature. At the outflow plane zero gradient boundary conditions are set for all quantities but the pressure, for which a fixed mean value is prescribed. The instantaneous results are averaged spatially in spanwise direction as well as over a period of approximately 100 flow through times.

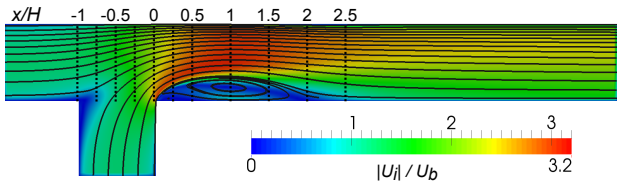

Figure 2. Mean flow streamlines and velocity magnitude normalized by the bulk velocity U_b obtained with the present VLES model.

The mean flow field arising from the impingement of the two crossing streams is displayed in Fig. 2. The flow detaches at $x/H = 0$, developing a recirculation zone at the lower wall with associated flow acceleration in the upper part of the channel and the resulting shear layer, responsible for strong turbulence production, in between. Further downstream at $x/H = 2$, the flow reattaches. In the following, flow and thermal field are evaluated quantitatively at different positions x/H marked by the dotted lines.

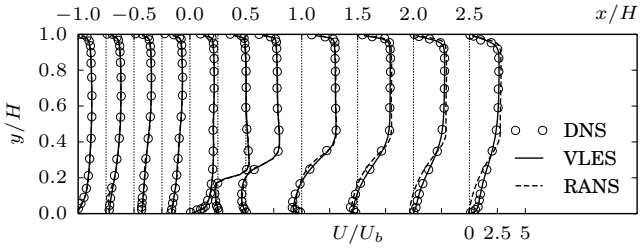

Figure 3. Velocity profiles normalized by the bulk velocity U_b at different positions x/H. DNS data taken from Hattori *et al.* (2014).

Fig. 3 shows the development of the mean streamwise velocity profiles. The VLES results follow closely the reference DNS data at all positions. This good agreement is also reflected by the prediction of the reattachment point at $x/H = 2.02$ compared to the DNS value of $x/H = 2.00$. The RANS simulation resulted in a too long recirculation zone, with reattachment occurring at $x/H = 2.69$. This is in agreement with the underestimation of the velocity underneath the separating shear layer, starting at $x/H = 1$. Development of the turbulent intensity profiles obtained by the VLES is displayed in Fig. 4. Overall good agreement between the VLES and DNS data can be observed, with a slight overprediction of the streamwise turbulent intensity near the top and bottom wall starting at $x/H = 1$.

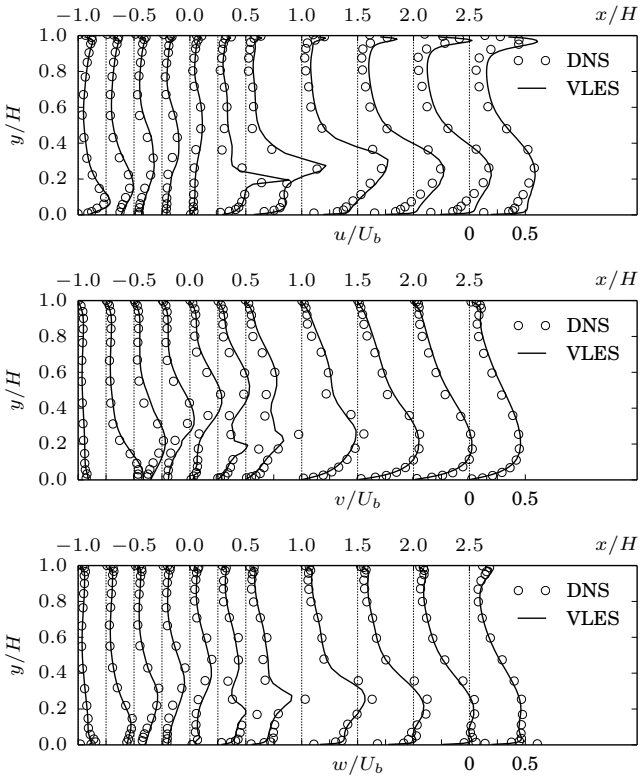

Figure 4. Turbulent intensity profiles in streamwise, wall-normal and spanwise directions, normalized by the bulk velocity U_b at different positions x/H. DNS data taken from Hattori *et al.* (2014).

Regarding the thermal field, mean temperature profiles and turbulent heat fluxes are analyzed. Fig. 5 shows the development of non-dimensionalized temperature profiles in streamwise direction. Thermal mixing is captured accurately in the VLES, with a minor tendency towards overprediction of the mixing process, resulting in a slightly underestimated temperature at the bottom wall at positions $x/H > 2.0$. In the RANS simulation however, thermal mixing is underpredicted resulting in a too narrow thermal mixing layer with corresponding underestimation of temperature in the lower and overestimation in the upper part of the channel. Non-dimensionalized turbulent heat flux profiles in streamwise and wall-normal directions for the VLES case are shown in Fig. 6. The shape of the profiles is captured correctly but a certain underestimation is noticeable at all positions, especially for the wall-normal turbulent heat flux.

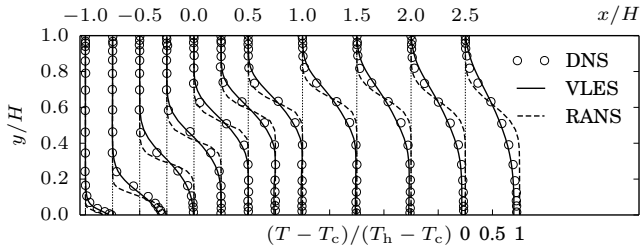

Figure 5. Temperature profiles normalized with hot and cold stream temperatures T_h and T_c at different positions x/H. DNS data taken from Hattori *et al.* (2014).

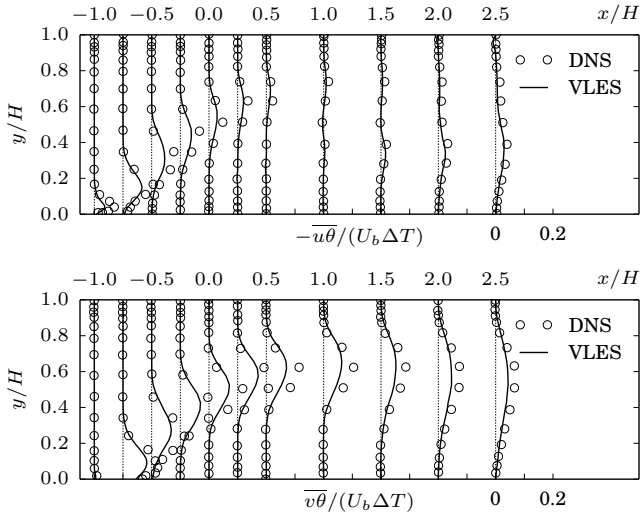

Figure 6. Turbulent heat fluxes in streamwise and wall-normal directions, normalized by the bulk velocity U_b and the temperature difference $\Delta T = T_h - T_c$ at different positions x/H. DNS data taken from Hattori *et al.* (2014).

VARIABLE PROPERTY FLOW IN A T-JUNCTION

Dimensions and flow conditions for the three-dimensional case comply with the reference experimental investigation conducted by Hirota *et al.* (2010). As in the previous case, the computational domain consists of two parts: the horizontal duct with dimensions $8H \times H \times 2H$ and the branch duct with $H/2 \times H \times 2H$. The mesh is refined towards top and bottom wall, as well as side walls. It consists of a $262 \times 75 \times 130$ cells in the main duct and $40 \times 40 \times 130$ cells in the branch duct, resulting in 2.762.500 cells in total. Inflow data is again generated by simultaneous precursor simulations. Temperature is set to a fixed value of $T_c = 12°C$ in the main duct and $T_h = 60°C$ in the branch duct, which corresponds to the values from the experimental investigations. This temperature difference entails density and viscosity variations of approximately 15% and 13%, respectively. Hence, temperature dependence of density and viscosity are taken into account in this case. Boundary conditions remain unchanged compared to the previous case, except that wall boundary conditions are applied at the sides. The instantaneous results are averaged over a period of 100 flow-through times.

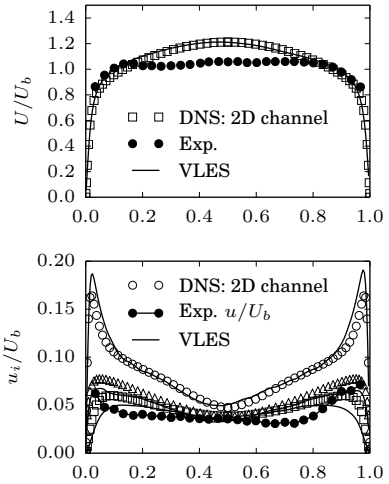

Figure 7. Velocity and turbulent intensities at the middle plane ($z/A = 0$) of the main inlet duct compared to DNS of channel flow at $Re_\tau = 395$ of Moser *et al.* (1999) and Exp. data by Hirota *et al.* (2010).

Fig. 7 shows the velocity profiles and turbulent intensities from the precursor simulations serving as inlet data for the main duct compared to DNS for plane channel flow at a similar Reynolds number (Moser *et al.*, 1999) as well as experimental data. The comparison to the channel DNS illustrates, that the VLES results in the middle plane correspond to fully developed turbulent flow, but deviate from the inflow data in the experimental investigations. Since most of the turbulence production occurs in the shear layer, inflow data is expected to be of minor importance. Furthermore, no experimental data for the branch channel is available, hence fully developed flow was used for both inlets.

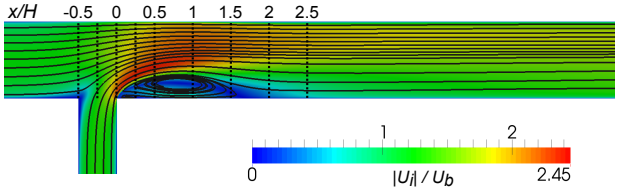

Figure 8. Streamlines and velocity magnitude normalized by the bulk velocity U_b in the $z/A = 0$ plane obtained with the present VLES model.

Fig. 8 displays streamlines and velocity magnitudes in the middle plane ($z/A = 0$) obtained with the present VLES model. As expected, the flow topology is qualitatively very similar to the pre-

vious case, with the formation of a recirculation zone and associated separation and reattachment of the flow. Dotted lines mark the positions x/H at which quantitative comparisons between the computational results and the reference experimental data are drawn.

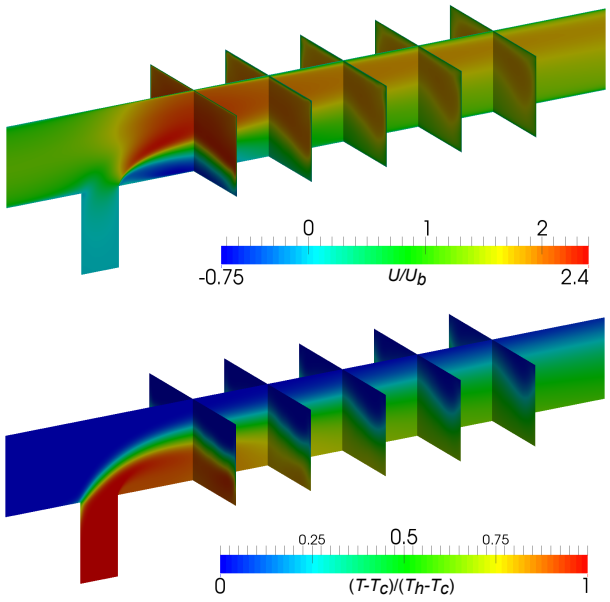

Figure 9. Mean streamwise velocity component (top) and temperature (bottom) obtained with the present VLES model.

The three-dimensional flow and thermal field is illustrated in Fig. 9 in terms of the normalized streamwise velocity component and the non-dimensionalized temperature on several planes in the computational domain. The flow is symmetric with respect to the middle plane and the influence of the side walls is noticeable in both the velocity and the temperature field.

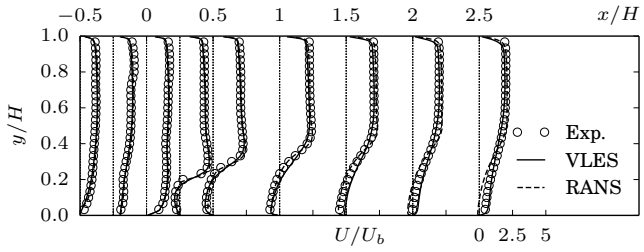

Figure 10. Velocity profiles normalized by the bulk velocity U_b at different positions x/H in the $z/A = 0$ plane. Exp. data taken from Hirota *et al.* (2010).

Fig. 10 shows the streamwise velocity profile development. The agreement between the computational results and the experimental data is similar to the quasi-two-dimensional configuration: the VLES results are in good agreement with the reference data while the RANS simulation shows minor deviations near the bottom wall, especially at the positions further downstream. Consequently, the prediction of the reattachment point is reasonable in the VLES with $x/H = 1.79$ compared to the experimentally obtained value of $x/H = 2$. In the RANS simulation the length of the recirculation zone is again overpredicted, with reattachment occurring at $x/H = 2.85$. Turbulent intensities in x and y-direction are shown in

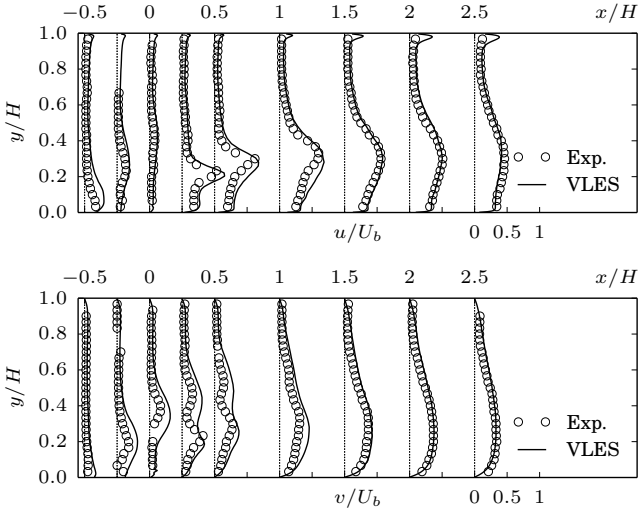

Figure 11. Turbulent intensity profiles in streamwise and wall-normal, normalized by the bulk velocity U_b at different positions x/H in the $z/A = 0$ plane. Exp. data taken from Hirota *et al.* (2010).

Fig. 11. In general, the profiles are in reasonable to good agreement with the reference data. The streamwise turbulent intensity is captured correctly with slight overestimation in the recirculation region at $x/H = 0.5$ and $x/H = 1$. The peaks in the vicinity of the top wall are not present in the experimental data set. However, qualitatively this behavior seems to be correct and the same effect is visible in the DNS data of the Hattori *et al.* (2014) case. The turbulent intensity in y-direction is captured less accurately compared to the streamwise fluctuations, especially in the region $-0.25 \leq x/H \leq 1$. While the shape of the profiles is qualitatively correct, the intensity is somewhat overpredicted. Possibly, the higher turbulence levels in the VLES, especially near the branch channel, are related to the deviations from the experimental inflow data (see Fig. 7). The higher turbulence intensity level in the separating shear layer, complying with a more intensive entrainment of the surrounding fluid in the recirculation zone, is in accordance with a somewhat shorter separation bubble. Overall, the mean flow field and turbulence statistics are in reasonable to good agreement with the reference data.

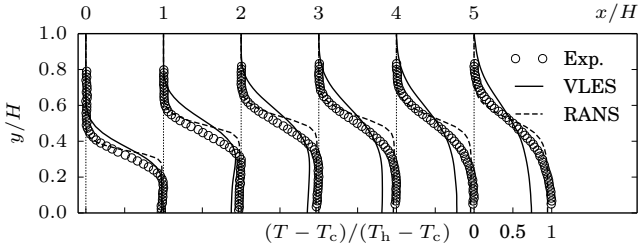

Figure 12. Temperature profiles normalized by hot and cold stream temperatures T_h and T_c at different positions x/H in the $z/A = 0$ plane. Exp. data taken from Hirota *et al.* (2010).

In regards to thermal mixing, mean temperature and turbulent heat fluxes are analysed. Fig. 12 shows the temperature profile development in streamwise direction. Clearly, both the VLES and RANS results show deviations from the reference data set. In the VLES case, the mixing is overestimated considerably, resulting in a more intensive spreading of the thermal mixing layer. At $x/H = 0$ the temperature is already overpredicted in the mixing layer. This

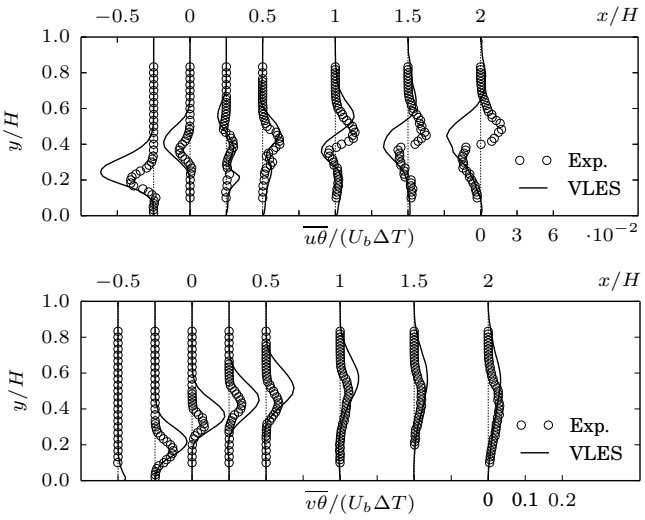

Figure 13. Turbulent heat fluxes in streamwise and wall-normal directions, normalized by the bulk velocity U_b and the temperature difference $\Delta T = T_\mathrm{h} - T_\mathrm{c}$ at different positions x/H in the $z/A = 0$ plane. Exp. data taken from Hirota *et al.* (2010).

trend continues further downstream resulting in an underestimation of the bottom wall temperature. The apparent superiority of the RANS results in regards to the prediction of the temperature field seem unlikely, considering the more accurate prediction of the flow field in the VLES. In the RANS simulation, the mixing seems to occur to slow resulting in a narrower thermal mixing layer, as it was the case in the quasi-two-dimensional configuration. However, contrary to the previous case, the bottom wall temperature is underpredicted despite the insufficient mixing. Fig. 13 shows the turbulent heat fluxes in x and y-direction. The magnitude of the streamwise turbulent heat flux is clearly overestimated at the position of the branch duct ($-0.5 \leq x/H \leq 0$). Further downstream, the predictions initially improve until $x/H = 1.5$, where the VLES results indicate heat flux mainly against the flow direction, while in the experiment heat flux in flow direction is observed in the upper part of the configuration. Turbulent heat fluxes in y-direction are in general overestimated, especially in the region $-0.25 \leq x/H \leq 1$. The position of the peak values are shifted upwards compared to the experimental data. The overestimation of the turbulent heat fluxes is consistent with the overprediction of the thermal mixing process.

CONCLUSIONS

The thermal mixing of flow-crossing streams in a T-shaped junction was studied computationally, applying a hybrid LES/RANS model based on the VLES concept. The residual turbulent motion is modeled using an elliptic-relaxations-based eddy viscosity model. For comparison purposes, simulations with the background RANS model were also performed. Two configurations were studied: a quasi-two-dimensional case with constant flow properties, for which DNS data was made available by Hattori *et al.* (2014), and a three-dimensional configuration subject to temperature dependent flow properties, which was investigated experimentally by Hirota *et al.* (2010). In the quasi-two-dimensional case, flow and thermal fields predicted with the VLES model exhibit very good agreement with the reference data base. Regarding the quality of the results, the VLES has a clear advantage over the RANS model, especially in terms of predicting the length of the recirculation zone and the thermal mixing process with the associated temperature distributions. The advantage of the VLES model is expected, since large turbulent structures are resolved in this hybrid LES/RANS scheme. For the three-dimensional configuration, the flow field is predicted reasonably well by the VLES model, with the most notable deviations from the reference data occuring in the prediction of the turbulent intensity in y-direction. The RANS model again overestimates the length of the recirculation zone by about 40%. The thermal field in the three-dimensional configuration is not predicted as accurately as in the quasi-two-dimensional case. The mixing process in the VLES is too strong resulting in too shallow temperature profiles and associated overprediction of the turbulent heat fluxes. The shortcomings in the prediction of the thermal fields in the three-dimensional configuration require further investigations, especially considering the reasonably accurate predicted flow field as well as the correct thermal field in the quasi-two-dimensional case. Further investigations will include a high fidelity LES to analyse the influence of the background RANS model, as well as studies concerning the influence of inflow data, the applied numerical schemes in the energy equation and the turbulent Prandtl number.

ACKNOWLEDGEMENTS

The financial support of the German Research Foundation (DFG) in the framework of the Collaborative Research Center/Transregio 150 (TP-B03) is gratefully acknowledged. The authors furthermore would like to thank for the computing time granted on the Lichtenberg HPC at TU Darmstadt.

REFERENCES

Chang, C.-Y., Jakirlić, S., Dietrich, K., Basara, B. & Tropea, C. 2014 Swirling flow in a tube with variably-shaped outlet orifices: an LES and VLES study. *Int. J. Heat and Fluid Flow* **49**, 28–42.

Hanjalić, K., Popovac, M. & Hadžiabdić, M. 2004 A robust near-wall elliptic-relaxation eddy-viscosity turbulence model for CFD. *Int. J. Heat and Fluid Flow* **25**, 1047–1051.

Hattori, H., Iwase, M., Houra, T. & Tagawa, M. 2014 DNS and LES for turbulent heat transfer and mixing in T-junction channel flow. *10th Int. ERCOFTAC Symp. on ETMM, Marbella, Spain* .

Hirota, M., Mohri, E., Asano, H. & Goto, H. 2010 Experimental study on turbulent mixing process in cross-flow type T-junction. *Int. J. Heat and Fluid Flow* **31**, 776–784.

Jakirlić, S., Kutej, L., Hanssmann, D., Basara, B. & Tropea, C. 2016 Eddy-resolving simulations of the notchback DrivAer model: influence of underbody geometry and wheels rotation on aerodynamic behaviour. *SAE Technical Paper 2016-01-1602* .

Kim, J. & Jeong, J. J. 2012 Large eddy simulation of turbulent flow in a T-junction. *Numerical Heat Transfer, Part A* **61**, 180–200.

Krumbein, B., Jakirlić, S. & Tropea, C. 2016 Jet impingement onto a heated wall: A VLES study. *11th Int. ERCOFTAC Symp. on ETMM, Palermo, Italy* .

Kuczaj, A. K., Komen, E. M. J. & Loginov, M. S. 2010 Large-eddy simulation study of turbulent mixing in a T-junction. *Nuclear Engineering and Design* **240**, 2116–2122.

Moser, R.D., Kim, J. & N.N., Mansour 1999 Direct numerical simulation of turbulent channel flow up to $\mathrm{Re}_\tau = 590$. *Physics of Fluids* **11** (4), 943–945.

Speziale, C. G. 1998 Turbulence modeling for time-dependent RANS and VLES: A review. *AIAA Journal* **36** (2), 173–184.

Sutherland, W. 1893 The viscosity of gases and molecular force. *Philosophical Magazine Series 5* **36** (223), 507–531.

Walker, C., Simiano, M., Zboray, R. & Prasser, H.-M. 2009 Investigations on mixing phenomena in single-phase flow in a T-junction geometry. *Nuclear Engineering and Design* **239**, 116–126.